Journal of Chromatography A, 1218 (2011) 4406–4416

Contents lists available at ScienceDirect

Journal of Chromatography A

journal homepage: www.elsevier.com/locate/chroma

Experimental investigation of the difference in B-term dominated band broadening between fully porous and porous-shell particles for liquid chromatography using the Effective Medium Theory

Anuschka Liekens, Joeri Denayer, Gert Desmet*

Vrije Universiteit Brussel, Department of Chemical Engineering, Pleinlaan 2, 1050 Brussels, Belgium

ARTICLE INFO

Article history:
Received 6 December 2010
Received in revised form 4 March 2011
Accepted 9 May 2011
Available online 14 May 2011

Keywords:
B-term
Longitudinal diffusion
Peak parking
Effective Medium Theory
Porous-shell particles

ABSTRACT

The difference in B-term diffusion between fully porous and porous-shell particles is investigated using the physically sound diffusion equations originating from the Effective Medium Theory (EMT). Experimental data of the B-term diffusion obtained via peak parking measurements on six different commercial particle types have been analyzed (3 porous and 3 non porous). All particles were investigated using the same experimental design and test analytes, over a very broad range of retention factor values. First, the B-term reducing effect of the solid core (inducing an additional obstruction compared to fully porous particles) has been quantified using the Hashin–Shtrikman expression, showing that the presence of a solid core can account for a reduction of about 11% when the core diameter makes up 63% of the total particle diameter (Halo and Poroshell-particles) and a reduction of 16% when the core diameter makes up 73% (Kinetex). Remaining differences can be attributed to differences in the microscopic structure of the meso-porous material (meso-pore diameter, internal porosity or relative void volume). The much lower B-term diffusion of Halo and Kinetex particles compared to the fully porous Acquity particles (some 20–40% difference, of which about 10–15% can be attributed to the presence of the solid core) can hence largely be attributed to the much smaller internal porosity and the smaller pore size of the meso-porous material making up the shell of these particles.

1. Introduction

In the pursuit of ever faster and more efficient liquid chromatography separations, many research efforts are currently being devoted to the study and the development of so-called superficially porous or porous-shell particles. This particle type was originally introduced by Kirkland in 1970 [1,2] and developed for the separation of large molecules. The concept appeared to be abandoned in the following decades, but has recently been re-introduced for the separation of small molecules by several manufacturers, with great success [3–7].

These newly introduced porous-shell particles display an excellent performance, with minimal plate heights often well below 2 [3,8,9], i.e., well below the assumed "magical" barrier for packed columns (although there is no ground to expect the existence of such a barrier [10]). These exceptionally low values could be partly attributed to a reduced C-term [4,8] and a reduced eddy-dispersion [8,11], in turn assumed to result from the very narrow particle size distribution with which these particles can be produced.

However, nearly all experimental studies also indicated a reduced B-term band broadening as one of the factors explaining the remarkably low minimal reduced plate heights. Typically, a 25% [8,11] to even a 40% reduction [4] of the B-term constant was observed. The B-term appears in any of the existing plate height expressions [12,13] and represents the part of the band broadening that is independent of the flow. As such, the most natural way to measure the B-term band broadening is by using the so-called peak parking method. This method was invented during the legendary 1962 taxi ride of Knox and Giddings [10,14,15]. In brief, a peak parking experiment consists of arresting the peak somewhere in the column (at a position far enough from the extremities) by stopping the flow for a given time t_{park}. After this period, the peak is then transported to the detector where its variance is measured. The purely symmetrical band broadening occurring during the parking period is then characterized by the peak spatial variance $\Delta\sigma^2{}_x$. According to theory, $\Delta\sigma^2{}_x$ can be expected to vary linearly with the parking time t_{park} [15–17]:

$$\Delta\sigma_x^2 = 2 \cdot D_{eff} \cdot t_{park} \quad (1)$$

The proportionality factor D_{eff} appearing in Eq. (1) is a measure of the effective longitudinal diffusion experienced by the analytes in a packed bed of (semi-)porous particles (Fig. 1). Inevitably, D_{eff} is a

* Corresponding author. Tel.: +32 02 629 32 51; fax: +32 02 629 32 48.
E-mail address: gedesmet@vub.ac.be (G. Desmet).

0021-9673/$ – see front matter © 2011 Elsevier B.V. All rights reserved.
doi:10.1016/j.chroma.2011.05.018

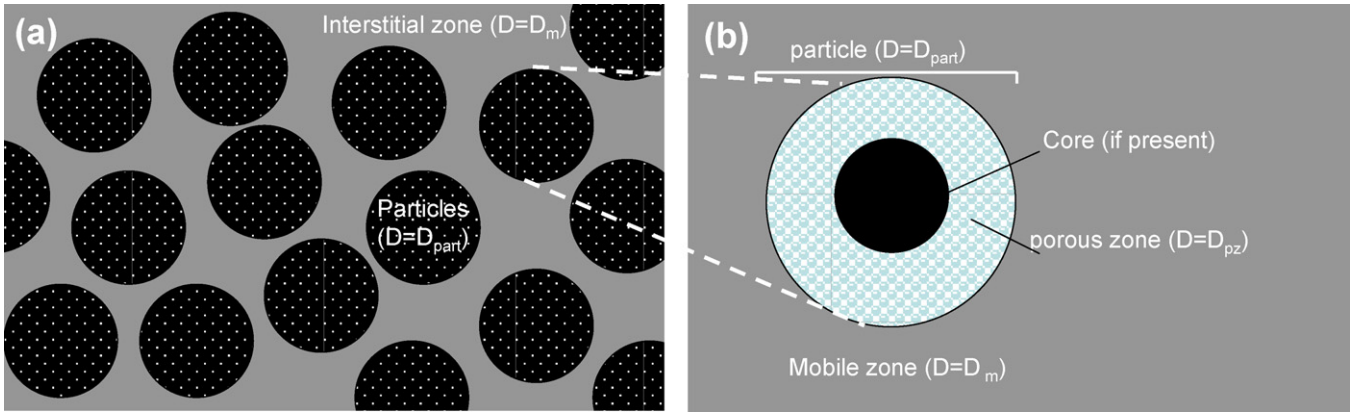

Fig. 1. Schematic representation of (a) the column viewed as a binary medium consisting of a discrete particle zone (with an over-all diffusion coefficient D_{part}) surrounded by a continuous interstitial void zone (with an diffusion coefficient D_m), (b) a zoom-in of the particle zone in the general case of a porous-shell particle containing a solid core surrounded by a meso-porous zone (with local diffusion coefficient D_{pz}).

combination of the diffusion rate in the mobile phase liquid outside the particles (determined by the bulk liquid molecular diffusion coefficient D_m) and that in the meso-porous space of the particles (determined by the intra-particle diffusion coefficient D_{part}). Obviously, if the column would only be filled with liquid, one would find that $D_{eff} = D_m$. If the column would only be filled with the particle material (no interstitial space), the peak parking measurement would yield $D_{eff} = D_{part}$. In general, D_{eff} is directly linked to the B-term plate height contribution via [15]:

$$H_B = \frac{2 \cdot D_{eff}}{u_0} \cdot (1 + k') \tag{2a}$$

$$\text{or (in reduced coordinates)}: \quad h_B = \frac{B}{\nu_0} = \frac{2 \cdot \gamma_{eff}}{\nu_0} \cdot (1 + k') \quad \text{with} \quad \gamma_{eff} = \frac{D_{eff}}{D_m} \tag{2b}$$

The present study has been set up to make an in-depth investigation of the observed differences in D_{eff}- or B-value between fully porous and porous-shell particles. An important difference with previous literature reports [8,9,11,18,19] is that the problem has been investigated using the Effective Medium Theory (EMT). This is a theory used in many other fields of science and technology to describe the effective conduction or diffusion in complex binary media [20–27]. In the field of chemical engineering, the EMT-approach has been used since long to model pure diffusion effects (i.e., in the absence of selective retention effects) in packed bed columns [28]. In the field of LC, the EMT-approach has already been used to estimate the diffusion in the meso-pore space as well as in the interstitial void of packed columns in the absence of retention [29]. Our group has recently adapted the EMT-expressions for use under retentive conditions in liquid chromatography [30,31].

2. Theory

As was shown in [30,31], the EMT-based expressions for longitudinal diffusion are much more accurate than the parallel-zone or residence-time weighted (RTW)-model that is traditionally used in the field of LC [4,8,11,16,17,32–35]. In fact, the RTW-model is in conflict with the general laws of diffusion (i.e., it breaks through the upper and lower bounds for diffusion in a binary medium) and introduces a false curvature in the relation between the observed intra-particle diffusion coefficient and the retention equilibrium constant [30,31]. On the other hand, even the most simple of all explicit EMT-expressions, i.e., the Maxwell-expression, is already accurate to within 5% over the entire range of typical diffusion and retention conditions that can be expected in reversed-phase LC [31,36]. Depending on the intra-particle diffusion rate, the Maxwell-model is even accurate to within 1% in the range of $0.1 < k' < 5.2$ for the case of $D_{part}/D_m = 0.5$, in the range of $1.6 < k' < 46.5$ for the case of $D_{part}/D_m = 0.1$ and in the range of $3.6 < k' < 93$ for the case of $D_{part}/D_m = 0.05$. Given that accuracies in the order of a few % are already much better than the expected experimental error, the present study only uses the Maxwell-based model. The reader is kindly referred to [31] for an overview of the more elaborate explicit EMT-models. Roughly speaking, these more elaborate models are only applicable to cases where the retention factor drops below $k' = 0.5$, a range that is anyhow of little practical importance. Implicit EMT-models, of which the Landauer–Davis model [20,21] is the most prominent example, are to be avoided because they lack any microscopic information about the bed geometry and only hold over a relatively narrow range of retention coefficients. Using the Landauer–Davis-model in its conventional form (i.e., with coordination number equal to 6), the model completely fails when approaching the non-porous particle packing case [31].

Using the Maxwell-based EMT-model and adapting it for use in liquid chromatography, the following expression for the B-term constant is obtained [31]:

$$B = 2 \cdot \frac{D_{eff}}{D_m} \cdot (1 + k') = \frac{2}{\varepsilon_T} \cdot \frac{1 + 2\beta_1(1 - \varepsilon_e)}{1 - \beta_1(1 - \varepsilon_e)} \tag{3}$$

In this expression, β_1 is the so-called particle polarizability constant [37]. For the case of spherical particles, β_1 is given by [31,38]:

$$\beta_1 = \frac{\alpha_{part} - 1}{\alpha_{part} + 2} \tag{4}$$

wherein α_{part} represents the relative permeability of the particles, relative with respect to the permeability of the mobile phase surrounding the particles, whose absolute permeability is simply equal to D_m. The physical meaning of the permeability coefficient of an analyte in a given medium is that it is the transport parameter linking the flux in chemical potential to its concomitant gradient [21], which is the single correct driving force for the transport in a binary medium displaying a partitioning equilibrium between both phases, as is the case in liquid chromatography. In dilute liquids, the permeability coefficient corresponds to the product of the diffusion coefficient and the partition coefficient this medium has with respect to a second medium it is in contact with.

As shown in [31], α_{part} depends on the ratio of D_{part} and D_m (definition: see Fig. 1a) as well as on a factor involving the retention factor k', and is given by:

$$\alpha_{part} = \frac{(1+k').\varepsilon_T - \varepsilon_e}{1-\varepsilon_e} \cdot \frac{D_{part}}{D_m} \quad (5)$$

wherein ε_T is the measured value of the total column porosity and ε_e is the interstitial void fraction or external porosity.

Another asset of the EMT is that it allows to isolate the effect of the solid core of porous-shell particles on the over-all longitudinal diffusion in a mathematically exact and 100% accurate way [31]. In general, the explicit EMT-models treat the column space as two distinct zones, a mobile zone (= interstitial zone outside the particles) and a particle zone consisting of individual spherical particles, as indicated in Fig. 1a. These particles are assumed to have uniform diffusion properties, generally represented by a particle-averaged diffusion coefficient D_{part}. As shown in [31,36], the EMT-expressions can, however, still be used, without any modification, when the particles are inhomogeneous and contain a solid core in their center. In this case, the D_{part}-expression takes the shape:

$$\frac{D_{part}}{D_{pz}} = \frac{2}{2+\rho^3} \quad (6)$$

wherein ρ is the ratio between the core diameter d_{core} and the particle diameter d_{part}. With reference to Fig. 1, it must be remarked that the D_{part}-parameter used in Eq. (6) represents the diffusion in a particle zone as observed by an external observer treating the particles as a black box medium with uniform properties, whereas D_{pz} is the intrinsic diffusion rate in the porous material making up either the shell of the particle (in case of porous-shell particles) or the full particle. If a column would be uniformly filled with shell-like material (i.e., a column without interstitial voids or solid cores), the effective diffusion coefficient D_{eff} one would measure via a peak parking experiment would be equal to D_{pz}. For fully porous particles, the difference between D_{part} and D_{pz} vanishes. This is clearly incorporated in Eq. (6), which returns that $D_{part} = D_{pz}$ when $\rho = 0$.

In the present study, a series of peak parking experiments were performed on six different columns packed with various fully porous or porous-shell particles (fully porous 1.7 μm Acquity particles, fully porous 3.5 μm Zorbax particles, fully porous 1.8 μm Eclipse particles, semi-porous 2.7 μm Halo particles, semi-porous 2.7 μm Poroshell particles and semi-porous 2.6 μm Kinetex particles). In each case, methylparaben was used as the test analyte. The analyte retention factor was varied by changing the fraction of methanol in the employed methanol/water mobile phase. For each particle type, the variation of the ratio D_{eff}/D_m as a function of the analyte retention factor k' has been investigated and Eqs. (3)–(6) have been used to isolate the effect of the solid core, and to estimate the contribution of the meso-pore and the stationary phase diffusion of the analyte.

3. Experimental

3.1. Chemicals and columns

Thiourea (MW = 76.12 g/mol), potassium iodide (MW = 166.01 g/mol), benzene (MW = 78.11 g/mol), toluene (MW = 92.14 g/mol), butylbenzene (MW = 134.22 g/mol) and methylparaben (MW = 152.15 g/mol) were provided from Sigma–Aldrich (Steinheim, Germany) and dissolved in the mobile phase at concentrations of 20 μg/ml for thiourea, 100 μg/ml for potassium iodide and 50 μg/ml for the other compounds. Methanol was of HPLC grade from Sigma–Aldrich (Steinheim, Germany). HPLC grade water was prepared in house using a Milli-Q Purification System (Millipore, Billerica, MA, USA). The Acquity BEH 1.7 μm C18 (2.1 mm × 100 mm) columns were purchased from Waters (Zellik, Belgium). The Zorbax StableBond 3.5 μm C18 (4.6 mm × 150 mm) columns were purchased from Agilent Technologies (Diegem, Belgium). The Zorbax RRHD Eclipse 1.8 μm C18 (3.0 mm × 100 mm) columns were provided by Agilent Technologies (Diegem, Belgium). The Halo 2.7 μm C18 (2.1 mm × 150 mm) columns were purchased from Advanced Materials Technology (Wilmington, USA). The Kinetex 2.6 μm C18 (4.6 mm × 100 mm) columns were provided by Phenomenex (Torrance, USA). The Poroshell 2.7 μm C18 (3.0 mm × 100 mm) columns were provided by Agilent Technologies (Diegem, Belgium). For each particle type, two columns were tested. Some of the most important geometrical parameters of the investigated particles and columns are given in Table 1. For the measurement of the molecular diffusion coefficient of the different water/methanol mobile phase compositions, a 2.1 mm × 100 mm column filled with non-porous 6.55 μm silica particles was provided by Thermo Fischer Scientific (Runcorn, UK). To conduct the total pore blocking experiments [11,39,40] an aqueous buffer was prepared that consisted of 10 mM ammonium acetate (Sigma–Aldrich, Steinheim, Germany) dissolved in Milli-Q water. The pH was adjusted to pH 3.0 by adding acetic acid (Panreac, Barcelona, Spain).

3.2. Apparatus

Chromatographic data were acquired with an HPLC Agilent 1200 system (Agilent Technologies, Waldbronn, Germany) which can deliver pressures up to 600 bar. This instrument includes an autosampler with a 2 μl loop, a diode array detector with a 2 μl flow cell, and a column oven which was set to 30 °C. Data acquisition, data handling, and instrument control were performed by Chemstation (Agilent Technologies). Absorbances were measured at 254 nm, using a constant rate of 40 Hz. Stainless steel tubing with an internal diameter of 120 μm and a length of 10.5 cm was used to connect the injector with the column. The column was connected to the 2 μl detector by stainless steel tubing with an internal diameter of 120 μm and a length of 40 cm.

3.3. Measurement of D_m and D_{eff}

In all peak parking experiments (those run on the non-porous column, as well as on the fully porous and the porous-shell particle columns), the effective diffusion coefficient was determined by stopping the mobile phase flow when the peak reached the middle of the column. The flow was stopped for a given time t_{park} = 0, 900, 1800, 2700 and 3600 s. During this time, the sample was allowed to diffuse freely in the column under the same experimental conditions. Afterwards the flow was resumed and the sample eluted trough the detector. Each experiment was performed in triplicate. The peak broadening was calculated using the following equation:

$$\sigma_t^2 = \frac{t_{tot}^2}{N} \quad (7)$$

where σ_t^2 is the peak variance, t_{tot} is the total retention time of the peak (t_R = elution time + parking time) and N is calculated by moment analysis with the Chemstation software. In a next step the temporal peak variance was transformed into spatial coordinates using:

$$\sigma_x^2 = \sigma_t^2 \cdot u_R^2, \quad (8)$$

wherein u_R is the linear velocity of the retained compound, calculated as $u_R = L/t_R$, with t_R the time needed to pass through the column with length L during the actual flow period (determined as $t_R = t_{tot} - t_{park}$). To correct the spatial peak variance for any other source of band broadening (the band broadening experienced during the time during which the peak is transported through the

Table 1
Overview of the geometrical characteristics of the considered particle types, including the particle diameter d_p, the ratio ρ between the core diameter d_c and the particle diameter, the total porosity ε_t, the external porosity ε_e and the porosity of the porous zone ε_{pz}. The measured and calculated values are the average of the results from the two columns tested for each particle type.

Name	d_p (μm)[a]	Pore size (Å)[a]	$\rho = d_c/d_p$[a]	Surface area (m^2/g)[a]	ε_e[b]	ε_t[b]	ε_{pz}[c]
Acquity	1.7	130	0	185	0.38	0.64	0.42
Zorbax	3.5	80	0	180	0.40	0.54	0.23
Eclipse	1.8	95	0	160	0.38	0.53	0.24
Halo	2.7	90	0.63	150	0.40	0.50	0.22
Kinetex	2.6	92	0.73	200	0.39	0.51	0.33
Poroshell	2.7	120	0.63	120	0.38	0.56	0.39

[a] Data taken from manufacturers documentation.
[b] Measured in house.
[c] Calculated using Eq. (14).

column and the extra-column parts, as well as the possible band broadening originating from the sudden halt and restart of the flow), the obtained σ_x^2-values were corrected by subtracting the σ_x^2-values obtained from an experiment wherein the peak was only arrested for 1 s. The thus obtained difference in peak variance $\Delta\sigma_x^2$ was plotted versus the applied parking time t_{park}. This plot shows a straight line and from the slope of this line the effective diffusion coefficient can be determined using Eq. (1).

As an alternative for the peak parking experiment, we also used "slow flow"-experiments as a verification of the measured D_{eff}-values. In these experiments, the peak is not stopped for a certain time, but the flow rate was adjusted such that the peak emerged from the column at a time similar to the total time in a peak parking experiment. This method has the advantage of not having to stop the flow when the peak reaches the middle of the column. This is important, because it cannot be excluded that stopping and restarting the flow has a disturbing effect on the resulting peak shape. The effective diffusion coefficient can then still be calculated from the linear relationship between $\Delta\sigma^2{}_x$ and t_R (obtained by replacing t_{park} by t_R in Eq. (1)).

To determine the molecular diffusion coefficient (D_m) of methylparaben in the different mobile phase mixtures considered here, peak parking measurements were conducted on a column packed with non-porous particles, with experimentally determined obstruction factor. This approach is similar to that used by Miyabe et al. [17] and is based on the fact that in a column packed with non-porous particles the effective diffusion factor derived from a peak parking experiment is always equal to:

$$D_{eff} = \gamma_{part}.D_m, \tag{9}$$

with γ_{part} being a geometric factor, independent of the test analyte or the mobile phase. To determine the value of γ_{part}, the column was tested using a number of test compounds and mobile phase compositions for which the value of D_m is well-known from the literature. The test compounds used were benzene in 100% methanol and 100% acetonitrile, toluene and butylbenzene in 50:50 v/v% water/methanol. The molecular diffusion coefficients of these compounds in their mobile phase compositions are known from the literature to be equal to 2.15×10^{-9} m^2/s, 3.73×10^{-9} m^2/s, 6.10×10^{-10} m^2/s and 5.39×10^{-10} m^2/s, respectively [41,42].

With this known value, we subsequently performed a series of peak parking experiments with methylparaben dissolved in the different mobile phases that were used to measure D_{eff} in the various fully porous and porous-shell particles columns. In all these experiments, the retention factor of methylparaben was varied by changing the volumetric percentage of methanol in the mobile phase from 20% to 55% in discrete steps.

The thus obtained D_m-values for methylparaben were subsequently compared to the predictions of D_m one can make using semi-empirical correlations such as the Wilke–Chang equation, the Carr equation and the Scheibel equation [41–43].

According to the Wilke–Chang equation [43], D_m is given by:

$$D_m = 74 \times 10^{-9} \frac{(\Phi_B M_B)^{1/2} \cdot T}{\eta_B \cdot V_A^{0.6}} \tag{10}$$

where Φ_B is the association factor of the solvent (1.9 and 2.6 for methanol and water, respectively [44,45]), T is the temperature, M_B the molecular weight of the solvent, V_A the molar volume of the solute and η_B the viscosity calculated using the following equation:

$$\eta_B = 10^{-2.429 + \frac{714}{T} - 1.859x + \frac{912}{Tx} + 1.8586x^2 - \frac{968}{Tx^2}} \tag{11}$$

where T is the temperature and x is the volume percentage of methanol in the mobile phase.

According to the Carr equation [42], D_m is given by:

$$D_m = 10^{-6}(-1 + AX - BX^2) \tag{12}$$

with: $X = ((M_B)^\alpha \cdot T/\eta_B^\beta \cdot V_A^\gamma)$, where $\alpha = 0.5$, $\beta = 1$, $\gamma = 0.6$ and A and B are taken to be 0.1531 and 0.000151, respectively. M_B is the molecular weight of the solvent. All the other symbols in the Carr equation have the same meaning as in the Wilke–Chang equation.

According to the Scheibel equation [41], D_m is given by:

$$D_m = \frac{82 \cdot 10^{-9} T}{\eta_B \cdot V_A^{1/3}} \left[1 + \left(\frac{3V_B}{V_A}\right)^{2/3}\right] \tag{13}$$

where V_B is the molar volume of the solvent. All the other symbols in the Scheibel equation have the same meaning as in the Wilke–Chang equation.

3.4. Measurement of the total and the external porosity

The total porosity ε_T can be readily calculated from the elution time of the unretained t_0-marker thiourea ($\varepsilon_T = F \cdot t_0/V_g$, where F is the applied flow rate and V_g is the geometrical volume of the column). For packed columns, it is usually a good approximation to assume that $\varepsilon_e = 0.38(\pm 0.02)$ with $\varepsilon_e = F \cdot t_i/V_g$, where t_i is the retention time of an analyte that only migrates through the interstitial void (thus the elution time that would be measured when injecting an analyte onto a column filled with non-porous particles). If desired, a more accurate value for ε_e can be obtained using ISEC or total pore blocking measurements [39,40,46–49].

Values of the external porosity ε_e have been measured using the so-called total pore blocking method [39,40]. Briefly, this method consists of filling the meso-pores of the particles with a hydrophobic liquid (decane in the present study) and then measuring the column residence time of an unretained ionic marker (potassium iodide) using an ammonium acetate buffer adjusted to pH 3.0. An essential step in obtaining an accurate estimate for ε_e is that the measured elution volume is corrected for all the extra-column volumes, including the volume of the column frits that usually correspond to some 0.01–0.02 external porosity units. This was done

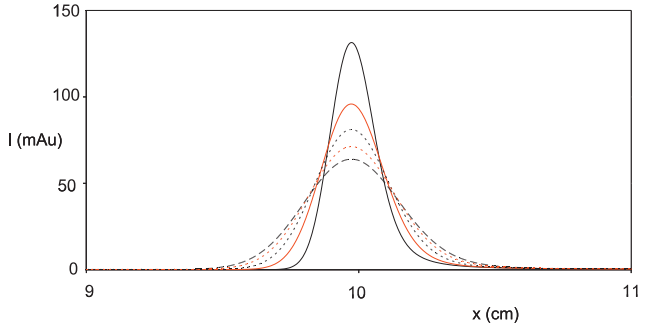

Fig. 2. Representation of the obtained peak shape for the peak parking experiment on the Acquity column for a 50/50 water/methanol mobile phase composition. The figure represents the signal intensity I as a function of the distance $\times$ traveled by the peak in the column. The peaks with parking time 0 s (full black line), 900 s (full red line), 1800 s (dotted black line), 2700 s (dotted red line) and 3600 s (dashed black line) are overlayed. (For interpretation of the references to color in this figure legend, the reader is referred to the web version of this article.)

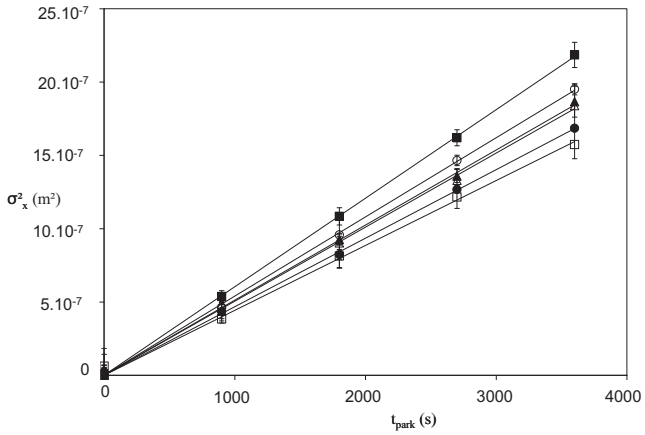

Fig. 3. Overview of the peak spatial variance σ^2_x as a function of the parking time t_{park} for the six particle types: Acquity (full squares), Zorbax (full triangles), Eclipse (full circles), Halo (open squares), Kinetex (open triangles) and Poroshell (open circles).

by measuring the mean residence time in a zero dead-volume connection piece and by correcting for the frit volumes. Correcting for the frit volumes was done using an empty column, identical to the column used for the measurement of the external porosity.

4. Results and discussion

4.1. Geometrical column and particle parameters

Table 1 shows the measured total (ε_T) and external porosities (ε_e), together with the internal porosity of the meso-porous zone ε_{pz} (shell layer in case of porous-shell particle, entire particle in case of fully porous particle). The latter (ε_{pz}) can be derived from the two former via [8]:

$$\varepsilon_{pz} = \frac{\varepsilon_T - \varepsilon_e}{(1-\varepsilon_e)\cdot(1-\rho^3)} \quad (14)$$

The estimated error on the obtained values is on the order of some 5%. The total porosity values for the Halo and Kinetex particles agree very well with recent values measured by Gritti et al. [11]. Also the significant difference in ε_{pz} between the Halo and the Kinetex particles agrees well with the observations made in [11]. The absolute ε_{pz}-values are slightly off, but this is due to the difference in measured external porosity. Mutually comparing the porous-shell particles, the Poroshell material has the largest local internal porosity (ε_{pz} = 0.39), while the Halo particles have a significantly smaller internal porosity (ε_{pz} = 0.22). The Kinetex particles have an intermediate internal porosity (ε_{pz} = 0.33). Another striking observation is the large difference in internal porosity between the fully porous particles, respectively, amounting up to ε_{pz} = 0.45 for the Acquity particles and only to ε_{pz} = 0.24 and 0.23 for the tested Zorbax Eclipse and Zorbax StableBond particles, respectively. The similar values obtained for the two latter particle types are in agreement with the fact that these particles are presumably made using similar methods.

Of each type of particles (fully porous and porous-shell), the particles with the largest local meso-porosity (ε_{pz}) are also the particles with the largest pore diameter (130 Å for Acquity and 120 Å for Poroshell).

4.2. Measurement of D_{eff} and D_m as a function of the mobile phase composition

Fig. 2 shows a set of peak parking bands obtained on one of the tested fully porous particle columns for different values of the parking time t_{park}. As can be noted, the peaks are symmetrical and broaden with increasing parking time, hence reflecting the effect of the time on the diffusive band broadening process. Similar results were obtained for the other considered mobile phase conditions and particle types. The highest peak is the reference peak, i.e., the one with negligible peak parking diffusion (t_{park} = 1 s). For a proper representation, the x-axis was transformed from temporal to spatial coordinates using the following transformation $x = (t - t_{tot})\cdot u_R$.

Fig. 3 subsequently shows how the difference in diffusion variance vary with increasing parking time for one given mobile phase composition and for the six different considered particle types. As can be noted, the data points for each particle type follow a nearly perfect straight line, in full agreement with Eq. (1). The difference in slope between the material producing the largest D_{eff}-value (Acquity, black squares) and that producing the lowest D_{eff}-value (Halo, open squares) is relatively large, of about 27%. For the other particle types, the difference in D_{eff}-value (and hence B-term constant) is less pronounced, and the straight line relationships obtained for the fully porous particles (full symbols) and porous-shell particles (open symbols) intermingle, clearly showing that the D_{eff}-value is not simply determined by the presence or the absence of a solid core.

The experiment represented in Fig. 3 was repeated for eight other mobile phase compositions. In each case, similar straight-line relationships as those shown in Fig. 3 were obtained. Eq. (1) was subsequently used to directly determine the value of D_{eff} from the slope of the best-fit straight line relationships. Fig. 4 combines all thus obtained D_{eff}-data and presents them as a function of the analyte retention factor k'. The error bars on the data points represent the upper and lower 95% confidence interval for the value of the slope of the curves in the experimental plots of $\Delta\sigma_x^2$ versus Δt_{park}.

As can be noted from Fig. 4, two of the porous-shell type particles (Halo and Kinetex) consistently produce the lowest D_{eff}-value (and hence B-term constant), whereas one of the fully porous particle types (Acquity) clearly leads to the highest D_{eff}-value. The Poroshell, Zorbax and Eclipse particles lead to comparable D_{eff}-values, situated between the already mentioned particle types. These observations clearly hold over a wide range of k'-values.

Since further analysis of the D_{eff} data based on Eqs. (3)–(6) requires the knowledge of the diffusion constant in the bulk mobile phase (D_m), a series of peak parking measurements was also conducted to determine the value of D_{eff} as a function of the fraction of organic modifier in the mobile phase in a column packed with

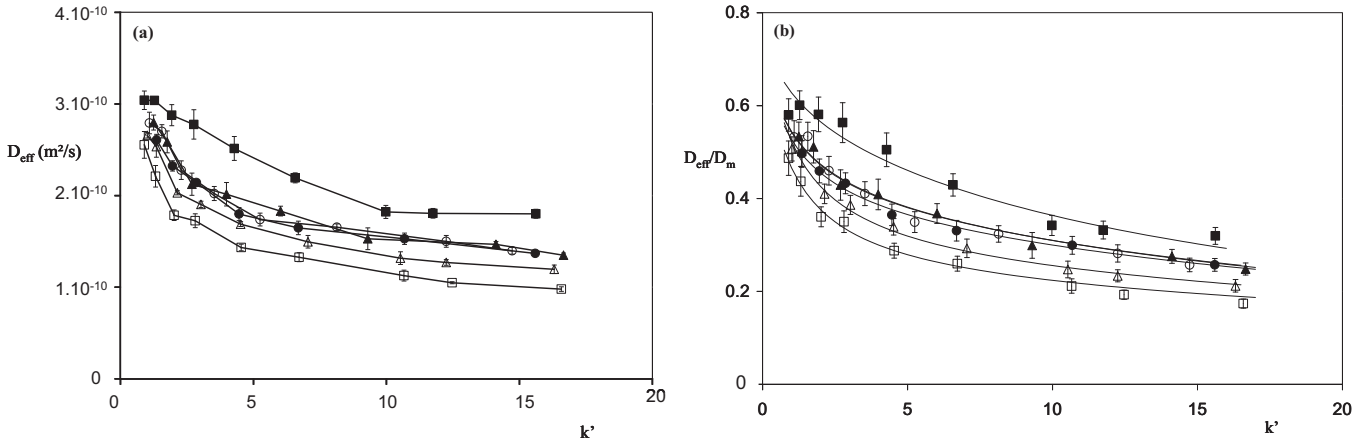

Fig. 4. (a) Variation of the measured effective diffusion D_{eff} as a function of the retention factor of methylparaben (k') for the six particle types. Same symbols as in Fig. 3. The full symbols correspond to the data points obtained with the fully porous particles and the open symbols correspond to the data points obtained with the porous-shell particles. Data points are connected for visualization purposes only. The error bars represent the 95% confidence interval on the value of the slope ($=2 \cdot D_{eff}$) of the straight line relationship between the experimental variances and the parking time, obtained via the linear regression analysis. (b) Variation of the corresponding D_{eff}/D_m ratio's.

non-porous particles with derived geometrical obstruction factor γ_{part}, as described in Section 3. Two types of experiments were conducted: peak parking experiments with select test compounds yielding $\gamma_{part} = 0.74$ (± 0.02) and "slow-flow" experiments yielding $\gamma_{part} = 0.72$. These two sets of values are in close agreement. Using an average value of $\gamma_{part} = 0.73$, based on Eq. (9), the peak parking measurements conducted to determine the D_m-value of methylparaben yielded a set of D_m-values as represented in Fig. 5. As can be noted, these are in a reasonably good agreement with the values predicted by the semi-empirical relationships that are available from the literature and discussed in Section 3.3 (Eqs. (10), (12) and (13)). From this plot, we can estimate the uncertainty on the measured D_m-values to be of the order of some 5–10%. When calculating the uncertainty on the measured D_m-values, it was found that the average error was of the order of some 5% (with a local minimum of 3% and a local maximum of 8%).

Fig. 5 also shows that the bulk diffusion coefficient of methylparaben varies only slightly across the range of mobile phase compositions investigated in this study. This explains why the graphical representation of the relation between D_{eff}/D_m versus k'

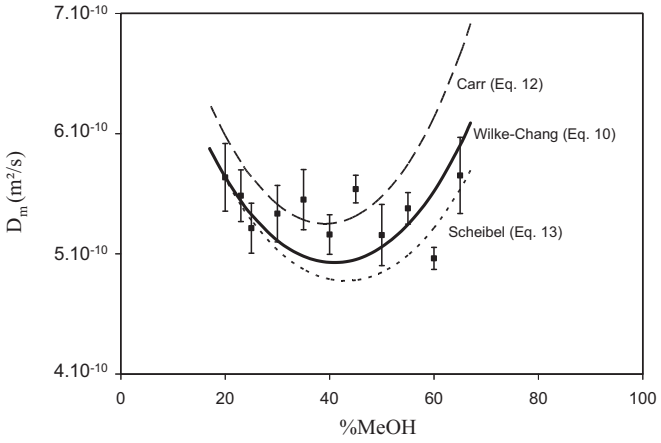

Fig. 5. Overview of the measured molecular diffusion D_m values (full squares) as a function of the percentage methanol in the mobile phase (%MeOH). The values calculated by the semi-empirical equations are added: Wilke–Chang (full line), Carr (dashed line) and Scheibel (dotted line).

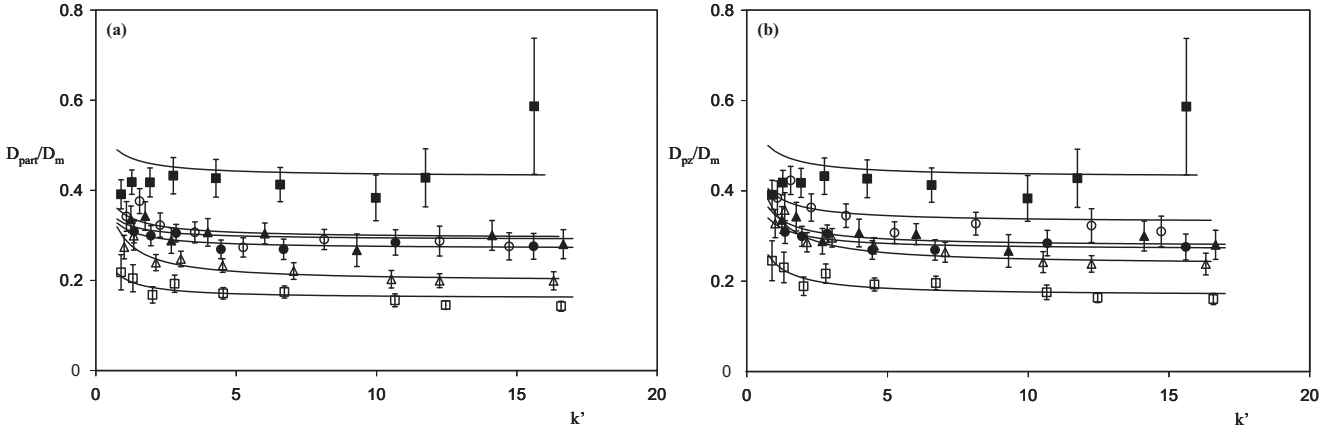

Fig. 6. (a) Variation of the measured ratio of the intra-particle diffusion coefficient and the molecular diffusion coefficient (D_{part}/D_m) values as a function of the retention factor of methylparaben (k') for the six particle types. Same symbols as in Fig. 3. The full symbols correspond to the data points obtained with the fully porous particles and the open symbols correspond to the data points obtained with the porous-shell particles. (b) Corresponding D_{pz}/D_m-data. The error bars represent the 95% confidence interval calculated via error propagation analysis. The full lines are calculated using the theoretical expressions given in the text (Eqs. (3) and (19)), with the assumption that the obstruction factor of the stagnant mobile phase in the pores of the particles equals its minimum possible value ($\gamma_{mp} = \gamma_{mp,min}$) and using the constant diffusion coefficient of methylparaben in the stationary phase ($\gamma_s D_s$) value represented by the horizontal lines in Fig. 7 (parameter values: see Table 2).

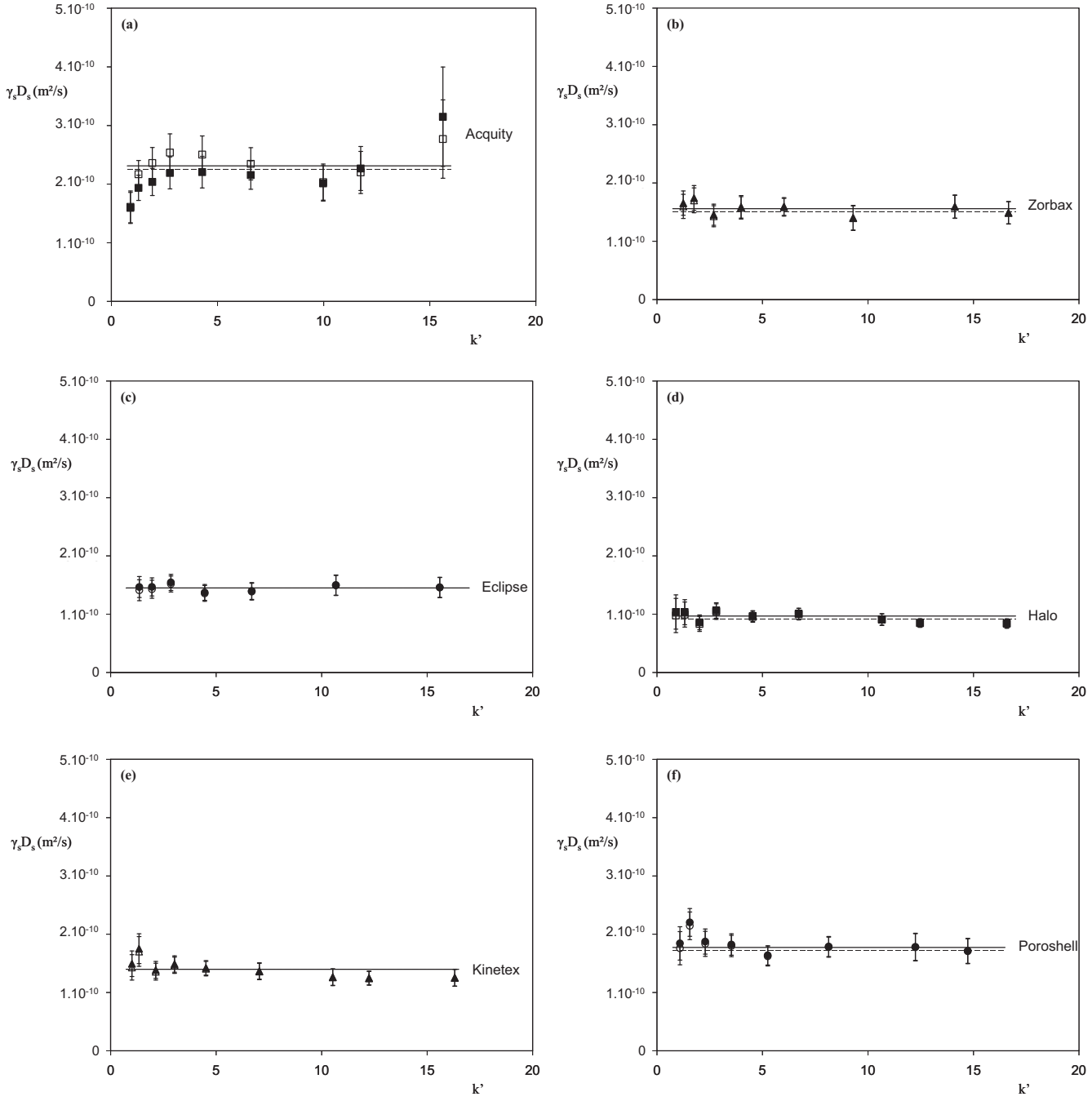

Fig. 7. Variation of the obtained values of the diffusion coefficient of methylparaben in the stationary phase ($\gamma_s D_s$) as a function of the retention factor of methylparaben (k') for the six particle types. (a) Acquity, (b) Zorbax, (c) Eclipse, (d) Halo, (e) Kinetex, (f) Poroshell. Full symbols: data obtained by assuming that $\gamma_{mp} = \gamma_{mp,min}$. Open symbols: data obtained by assuming that the obstruction factor of the stagnant mobile phase in the pores of the particles equals its maximum possible value ($\gamma_{mp} = \gamma_{mp,max}$). The error bars represent the 95% confidence interval calculated via error propagation analysis.

(Fig. 4b) looks very similar to the plot of D_{eff} versus k' shown in Fig. 4a.

4.3. Determination of D_{part} and D_{pz} using the observed D_{eff}-values

The first step in achieving a deeper understanding of the relationship between particle morphology and the observed D_{eff}-values obviously should be the elimination of the contribution of the diffusion experienced by the analytes when residing outside the particles. In other words, one should try to derive D_{part} from observed D_{eff} values. For this purpose, a sound model representing the relationship between both parameters is needed. The Maxwell-model represented by Eqs. (3)–(5) is such a model. Using the known values of D_{eff}/D_m (obtained by dividing the experimental D_{eff}-data shown in Fig. 4a by the corresponding D_m-value given in Fig. 5), Eq. (3) can be rewritten to first find the value of the corresponding polarizability constant β_1 (with $\gamma_{eff} = D_{eff}/D_m$):

$$\beta_1 = \frac{1}{1-\varepsilon_e} \cdot \frac{\gamma_{eff}\varepsilon_T(1+k') - 1}{2 + \gamma_{eff}\varepsilon_T(1+k')} \quad (15)$$

Subsequently using this value in Eq. (4), it is straightforward to find the corresponding α_{part}-value as:

$$\alpha_{part} = \frac{1+2\beta_1}{1-\beta_1} \tag{16}$$

From which, according to Eq. (5), the pursued D_{part}-value is then given by:

$$\frac{D_{part}}{D_m} = \frac{\alpha_{part}(1-\varepsilon_e)}{\varepsilon_T(1+k')-\varepsilon_e} \tag{17}$$

The thus obtained values for D_{part}/D_m are all given in Fig. 6a. A first observation that can be made from Fig. 6a is that the D_{part}/D_m-values vary less strongly with k' than the D_{eff}/D_m-values (see Fig. 4b). This decreasing trend observed in Fig. 4b is due to the fact that, with increasing k', the analytes spent progressively more and more time in the (slow) diffusion zone inside the particles and less in the (fast) diffusion zone outside the particles. Obviously, this effect is no longer present in Fig. 6a since there only the diffusion rate inside the particles is represented. A second observation from Fig. 6a is that a similar order as that observed in Fig. 4 is obtained: the Acquity particles (fully porous) lead to the highest D_{part}-values whereas the Kinetex and the Halo particles (porous-shell) lead to the lowest D_{part}-values. The other three particle types lead to intermediate and fairly similar D_{part} values. The origin of the added model curves is discussed in Section 4.4.2. The very large error bar for the highest k'-value of the Acquity data is due to the fact that the corresponding β_1-value lies close to unity. As can be noted from Eq. (16), where the denominator is given by $(1-\beta_1)$, this may lead to a large uncertainty on the α_{par}- and hence also on the D_{part}-value.

The next obvious step in the analysis of the (potential) difference between the fully porous and the porous-shell particles is investigating to what extent the observed D_{part}-values are influenced by the presence of the solid core in case of the three porous-shell particle types. For this purpose, Eq. (6) was used to calculate the corresponding D_{pz}-values, representing the diffusion in the actual meso-porous zone. For the fully porous particles, this changes nothing, since $D_{part} = D_{pz}$ when $\rho = 0$ in Eq. (6). For the porous-shell types, Eq. (6) shows that the core leads to a reduction of the apparent particle diffusion coefficient (D_{part}) compared to the diffusion coefficient (D_{pz}) describing the diffusive transport in the shell material by some 11% when the core diameter makes up 63% of the total particle diameter (Halo and Poroshell-particles) and by 16% when the core diameter makes up 73% (Kinetex particles). These values can be used with full confidence, since Eq. (6) can be derived in a strictly mathematically rigorous way [38] and has been validated numerically for all possible conditions one can expect in reversed-phase LC [36].

The differences observed between Fig. 6a (apparent diffusion coefficient inside the particles) and Fig. 6b (true diffusion coefficient inside the meso-porous shell) can now readily be understood. The data points for the fully porous particles remain unaltered, whereas the data points for the porous-shell particles shift some 10–15% upward. Despite this upward shift, the particles providing the lowest overall B-term diffusion (Halo and Kinetex) remain at the bottom of the graph, while the particles leading to the largest B-term diffusion are also the ones present in the top of the graph. This indicates that the major part of the difference in B-term diffusion (or equivalently, the main difference in D_{eff}-value) observed in Fig. 4a is due to a difference in the intrinsic diffusion properties of the meso-porous material and not due to the presence of the solid core (which, as explained in the above paragraph, only has a relatively small effect).

This shows that, by making fully porous particles out of the same material as the current porous-shell particles (i.e., with equally small D_{pz}) it would be possible to obtain fully porous particle columns with a reduced B-term contribution.

4.4. Determination of γ_{mp} and $\gamma_s D_s$ using the determined D_{pz}-values

Going one level deeper in the analysis, it should now be investigated how the D_{pz}-values shown in Fig. 6b can be related to the microscopic material parameters of the different particle types. Using the traditional assumption that the diffusion in the stagnant mobile phase and the diffusion experienced by the analytes when retained in or on the stationary phase occurs in parallel [50], and that both transport processes can be described by considering obstruction factors (γ_{mp} for the stagnant mobile phase and γ_s for the stationary phase, respectively), the combined diffusion coefficient can be written as [31]:

$$D_{pz} = \frac{\varepsilon_{pz}\gamma_{mp}D_m + (1-\varepsilon_{pz})\cdot K_{A,pz}\gamma_s D_s}{\varepsilon_{pz} + (1-\varepsilon_{pz})\cdot K_{A,pz}} \tag{18}$$

wherein $K_{A,pz}$ is the solid phase-based equilibrium constant representing the intrinsic thermodynamic retention equilibrium between the mobile phase liquid and the "non-liquid" part (stationary phase) of the meso-porous zone of the particles. The value of $K_{A,pz}$ can readily be calculated from the observed value of the analyte retention factor k' using [11,31]:

$$K_{A,pz} = \frac{\varepsilon_T}{(1-\varepsilon_e)\cdot(1-\rho^3)\cdot(1-\varepsilon_{pz})}k' \tag{19}$$

wherein $\rho = 0$ for fully porous particles.

In a recent publication [50], the stationary phase obstruction factor (γ_s) has already been incorporated into the reported D_s-value. In the present study, it has been preferred to keep the $\gamma_s D_s$-notation, as this is the notation used in most literature references [15,33,51] (note that $\gamma_s = 1/\tau_{surf}$ in [51]). The distinction between $\gamma_s D_s$ and the lumped D_s is irrelevant as γ_s and D_s cannot be measured separately.

The major problem encountered when trying to find the reason why a given observed D_{pz}-value is either low or high is that there are two unknowns (γ_{mp} and $\gamma_s D_s$) for one known value (D_{pz}). Two approaches can be proposed to overcome this. In the first, most frequently used approach, one can use one of the existing geometrical models to estimate the value of γ_{mp}, so that the $\gamma_s D_s/D_m$-value can then be directly derived. In the second approach, one can try to fit Eq. (18) to the experimental data shown in Fig. 6b by varying the value of γ_{mp} and $\gamma_s D_s/D_m$. In the present study, both approaches have been used (see Sections 4.4.1 and 4.4.2, respectively) and mutually compared.

4.4.1. Determination of $\gamma_s D_s$ from the D_{pz}-data presented in Fig. 6b using an estimated value of γ_{mp}

To determine $\gamma_s D_s$ using Eq. (18), first an estimate the meso-pore obstruction factor γ_{mp} is needed. Generally, γ_{mp} is calculated as the product of the diffusion hindrance factor $F(\lambda)$ and the meso-pore obstruction factor γ_{np} [34]:

$$\gamma_{mp} = \gamma_{np}\cdot F(\lambda) = \frac{F(\lambda)}{\tau_{pz}^2} \tag{20}$$

In some literature also expressed in terms of the pore tortuosity τ_{pz}, via $= 1/\tau^2{}_{pz}$. In Eq. (20), $F(\lambda)$ is the pore hindrance factor, with λ being the ratio of the molecular diameter of the analyte to the pore diameter. $F(\lambda)$ turns to unity (no hindrance) when λ turns to zero. Giddings [52] also considered a pore constriction factor that should be multiplied with the factors already appearing on the right hand side of Eq. (20). However, in the recent publication, this seems to be neglected, probably because of the improved meso-pore structure of modern HPLC particles.

First focussing on the value of γ_{np}, it should be considered that most correlations that exist to predict the value of γ_{np} are based on the assumption that the meso-porous zone can be represented as a packing of non-porous nano-spheres. Again, the EMT provides a set of different expressions (with varying degree of complexity and accuracy) that can be used to estimate γ_{np}. An overview is given in [36]. As already mentioned in Section 1, the most simple of all EMT-models is the Maxwell-based model. In its non-porous particle limit, this model reduces to [36]:

$$\gamma_{np} = \frac{1}{\tau_{pz}^2} = \frac{2}{3 - \varepsilon_{pz}} \tag{21}$$

More detailed expressions can be derived from the EMT when bringing higher order terms into account. As shown in the numerical study presented in [36], a highly accurate estimation of γ_{np} can be obtained by starting from the Cheng and Torquato-model [36]. The non-porous particle limit of this expression is given by (after filling in the value of the effective porosity of the meso-porous zone ε_{pz}):

$$\gamma_{np} = \frac{1}{\tau_{pz}^2} = \frac{2 - \zeta_2}{3 - \varepsilon_{pz}(1 + \zeta_2)} \tag{22}$$

wherein ζ_2 is the so-called three-point parameter. As can be noted, Eq. (22) is the higher order variant of the Maxwell model given by Eq. (21). When $\zeta_2 = 0$, Eq. (22) simplifies to Eq. (21). The values of the ζ_2-parameter can be calculated using either the correlation obtained in [53] for ordered face-centered cubic packing of spheres (range of validity: $0.25 < \varepsilon_{pz} < 1$):

$$\zeta_2 = 0.0237(1 - \varepsilon_{pz}) - 0.434(1 - \varepsilon_{pz})^2 + 2.5318(1 - \varepsilon_{pz})^3 - 5.7176(1 - \varepsilon_{pz})^4 + 5.1187(1 - \varepsilon_{pz})^5 \tag{23a}$$

Or that obtained in [38] for a random packing of spheres (range of validity $0.4 < \varepsilon_{pz} < 1$):

$$\zeta_2 = 0.21068(1-\varepsilon_{pz}) - 0.0469(1-\varepsilon_{pz})^2 + 0.00247(1-\varepsilon_{pz})^3 \tag{23b}$$

Eq. (23b) returns a value of $\zeta_2 = 0.11$ for the case of $\varepsilon_{pz} = 0.38$. This is in close agreement with numerical calculations presented in [53], yielding a value of $\zeta_2 = 0.13$. For the same porosity, Eq. (23a) yields a value of $\zeta_2 = 0.075$.

Still considering Eq. (20), but now focussing on the pore hindrance factor $F(\lambda)$, it should be noted that also various expressions exist in the literature to calculate $F(\lambda)$, each having their own range of applicability and degree of accuracy [54,55]. Three of the most frequently used expressions, obtained by calculating the drag force experienced by a spherical particle when moving near a solid wall are given here below:

$$F(\lambda) = \frac{1 + (9/8)\lambda \ln \lambda - 1.539\lambda}{1 - 2\lambda + \lambda^2} \quad \text{(Brenner and Gaydos)} \tag{24a}$$

$$F(\lambda) = \frac{1 - 2.105\lambda + 2.0865\lambda^3 - 1.7068\lambda^5 + 0.7260\lambda^6}{1 - 0.75857\lambda^5} \quad \text{(Haberman)} \tag{24b}$$

$$F(\lambda) = (1 - \lambda^2)(1 - 2.1044\lambda + 2.089\lambda^3 - 0.948\lambda^5) \quad \text{(Renkin,} \quad \lambda > 0.1) \tag{24c}$$

As can be noted from Table 2, each of these yields a slightly different values for $F(\lambda)$. If desired, one can make more detailed calculations to account for the spread in meso-pore sizes [11]. This approach has not been adopted here, because it is believed that the values returned by any of the available $F(\lambda)$-expressions are anyhow highly uncertain because they are based on the assumption of a solid sphere moving near the solid wall of a cylindrical tube, which is anyhow just a crude representation of the reality. Using a commercial structure builder program (Gaussview 3.0, Gaussian Inc., Wallingford, CT), the distance between the two most remote hydrogen atoms can be calculated to be 9.2 Å, whereas the shortest distance across the molecule is some 5.1 Å large. Taking the

Table 2
Measured values of the porosity of the porous zone ε_{pz} and derived estimates for the obstruction factor of the stagnant mobile phase in the pores of the particles γ_{mp} and the ratio of the diffusion coefficient of methylparaben in the stationary phase and the molecular diffusion coefficient ($\gamma_s D_s/D_m$). The minimal, maximal and fitted values of these parameters are given with subscript min, max and fit, respectively. The diffusion hindrance factor $F(\lambda)$ and the tortuosity factor of the porous zone τ_{pz} calculated using different approaches are also given in the table. For the origin of the data, see text.

Particle type	ε_{pz}	$F(\lambda)$ Brenner & Gaydos	$F(\lambda)$ Habermann	$F(\lambda)$ Renkin	$1/\tau_{pz}^2$ Maxwell	$1/\tau_{pz}^2$ Torquato-fcc	$1/\tau_{pz}^2$ Torquato-rand	$\gamma_{mp,min}$	$(\gamma_s D_s/D_m)_{min}$	$\gamma_{mp,max}$	$(\gamma_s D_s/D_m)_{max}$	$\gamma_{mp,fit}$	$(\gamma_s D_s/D_m)_{fit}$
Acquity	0.42	0.79	0.85	0.85	0.78	0.77	0.76	0.60	0.43	0.65	0.42	0.63	0.43
Zorbax	0.23	0.69	0.76	0.75	0.74	0.68	0.70	0.47	0.29	0.52	0.28	0.62	0.28
Eclipse	0.24	0.73	0.80	0.79	0.73	0.66	0.69	0.48	0.27	0.53	0.27	0.53	0.27
Halo	0.22	0.72	0.79	0.78	0.73	0.67	0.69	0.48	0.18	0.53	0.17	0.60	0.17
Kinetex	0.33	0.72	0.79	0.78	0.76	0.74	0.73	0.54	0.26	0.59	0.85	0.59	0.24
Poroshell	0.39	0.77	0.84	0.83	0.77	0.75	0.74	0.58	0.33	0.63	0.32	0.75	0.30

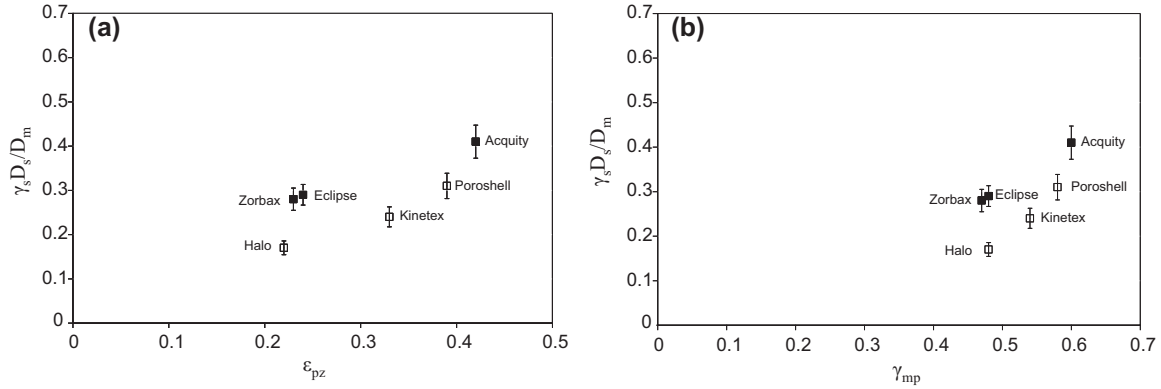

Fig. 8. (a) Overview of the measured ratio of the diffusion coefficient of methylparaben in the stationary phase and the molecular diffusion coefficient ($\gamma_s D_s/D_m$) values (squares) as a function of the porosity of the porous zone ε_{pz} for the six different columns. (b) Overview of the measured ratio of the diffusion coefficient of methylparaben in the stationary phase and the molecular diffusion coefficient ($\gamma_s D_s/D_m$) values (squares) as a function of γ_{mp} for the six different columns.

largest dimension (9.2 Å), in combination with the nominal value of the pore diameter of the different particles, the λ-values shown in Table 2 are obtained.

Given the important assumptions (hard sphere interaction with the pore walls, pores treated as cylindrical tubes) underlying the calculation of $F(\lambda)$, one can assume that there is some uncertainty of about 10–20% to its value (as will be shown later on, exactly knowing the value of γ_{np} and $F(\lambda)$ is anyhow only important to predict the B-term constant for very early eluting components ($k' < 1$)).

Table 2 shows the different γ_{np}- and $F(\lambda)$-values that are obtained from the above presented correlations, using the respective values of the pore size and the ε_{pz}-value of each particle type (see Table 1 for corresponding values). With the three different values for γ_{np} and the three different values for $F(\lambda)$, in total six different values for γ_{mp} can be obtained from Eq. (20). To limit the number of considered cases, only the combination leading to the lowest and the highest γ_{mp}-value (resp. denoted by $\gamma_{mp,min}$ and $\gamma_{mp,max}$) have been considered and are represented in Table 2. As will be noted further on, the difference between the minimum and the maximum values is anyhow so small that an investigation of the intermediate γ_{mp}-values would be superfluous. The model curves added to Fig. 6 were calculated for the case of $\gamma_{mp} = \gamma_{mp,min}$, it was found that the model curves obtained by taking $\gamma_{mp} = \gamma_{mp,max}$ only differed minimally.

Both γ_{mp}-values ($\gamma_{mp,min}$ and $\gamma_{mp,max}$, see Table 2) have subsequently been used in combination with Eq. (18) to estimate the value of $\gamma_s D_s/D_m$ from the experimental D_{pz}-values presented in Fig. 6b:

$$\frac{\gamma_s D_s}{D_m} = \frac{D_{pz}/D_m[\varepsilon_{pz} + (1-\varepsilon_{pz})\cdot K_{A,pz}] - \varepsilon_{pz}\gamma_{mp}}{(1-\varepsilon_{pz})\cdot K_{A,pz}} \quad (25)$$

with $K_{A,pz}$ given by Eq. (19).

The obtained values are given in Fig. 7a–e. As can be noted, the $\gamma_s D_s/D_m$-values obtained for the $\gamma_{mp,min}$- and the $\gamma_{mp,max}$-case only differ very little. This is in agreement with the fact that the second term in the numerator of Eq. (18) dominates the first term over most of the considered k'-range because of the large $K_{A,pz}$-value. This is in agreement with the statements in [16,50] saying that in reversed phase LC the analytes essentially migrate through the particles via the diffusion in the stationary phase. As a consequence, the value of γ_{mp} only has a poor effect on the finally obtained values for $\gamma_s D_s/D_m$. The value of γ_{mp} only becomes the dominant contributor to D_{pz} when $K_{A,pz}$ becomes small, i.e., when k' tends to zero. In this case, the adopted value for γ_{mp} starts to have an influence on the calculation. In Fig. 7a–e, this is reflected by the fact that the difference between the two calculated $\gamma_s D_s$-values is consistently larger for the smallest k'-points.

An interesting observation that can be made from Fig. 7 is that $\gamma_s D_s/D_m$ varies only very weakly with k'. In fact, the obtained data only allow to conclude that $\gamma_s D_s/D_m$ is independent of the retention equilibrium or k'. This is in contrast with earlier observations reported in the literature [50], reporting a clear decrease of $\gamma_s D_s$ with k'. Obviously these literature results were obtained using the parallel-zone or RTW-model, which is known to introduce a false additional curvature in the observed relation between $\gamma_s D_s$ and k' [31,56]. The apparent constancy of the obtained $\gamma_s D_s$-data needs to be further investigated using different temperatures, mobile phases and analytes.

4.4.2. Determination of γ_{mp} and $\gamma_s D_s$ via direct fitting of the D_{pz}-data presented in Fig. 6b

Since the direct calculation of $\gamma_s D_s$ in the preceding section lead to values of $\gamma_s D_s$ that are, within the experimental error margin (as indicated by the error bars added to Fig. 7), independent of the value of k', it is also relatively straightforward to determine a value for γ_{mp} and $\gamma_s D_s$ by performing a two-parameter fitting of Eq. (18) to the D_{pz}-data shown in Fig. 6b (and assuming that $\gamma_s D_s$ is a constant, independent of k'). The fitting was carried out using the Solver function of MS® Excel 2003, using the average of the values obtained for γ_{mp} and $\gamma_s D_s$ in the previous section as the starting values for the fitting algorithm. The thus obtained γ_{mp}- and $\gamma_s D_s$-values are given in Table 2 (last two columns). As can be noted, the obtained values differ only minimally from those obtained with the previous method. In addition, the corresponding fitted curves for D_{pz} and D_{part} (see black full line curves added to Fig. 6a and b) represent the measured data very well, except for the Acquity data (top curve). In this case, the scatter on the measurements is, however, very large, making it difficult to make a conclusive statement about the quality of the fitting.

4.4.3. Correlation between the observed $\gamma_s D_s$-data and the microscopic material parameters

From the above analysis, it has become clear that part of the low B-term constant values observed for Halo and Kinetex is due to their low $\gamma_s D_s$-values (as this is the main contributor to D_{pz} over most part of the k'-range). Similarly, part of the large B-term constant values of the Acquity particles is due to their high $\gamma_s D_s$-values. Trying to correlate the observed $\gamma_s D_s$-data to the available microscopic material data (internal porosity of the meso-porous material ε_{pz} and the pore diameter) is, however, not straightforward since $\gamma_s D_s$ will certainly also be influenced by other parameters such as the microscopic quality of the surface chemical modification.

Nevertheless, taking the $\gamma_s D_s/D_m$-values obtained via the direct fitting method (see Section 4.4.2) and plotting them versus the

internal porosity (Fig. 8a), one observes a weak correlation between the diffusion in the stationary phase and the fraction of the internal meso-pore volume. This is in line with previous arguments saying that the diffusion in the stationary phase is also subjected to a similar type of obstruction as the diffusion in the mobile phase filling up the meso-pores [15,52,57]. The Zorbax and Eclipse data, however, make a clear exception to the observed correlation, as they produce a significantly larger $\gamma_s D_s$-value than the Halo-particles, whereas the materials have about the same internal porosity ε_{pz}.

Since ε_{pz} only incorporates part of the information about the microscopic material composition (it says nothing about the pore diameter), Fig. 8b shows a plot of $\gamma_s D_s/D_m$ versus γ_{mp}, as the latter incorporates information about both ε_{pz} and the pore diameter (cf. Eq. (20)). The new plot, however, changes nothing fundamental about the observations made from Fig. 8a: there is a weak trend between the diffusion in the stationary phase and the meso-pore diffusion, but some notable exceptions exist, notably for the Zorbax and Eclipse data.

5. Conclusions

Performing peak parking measurements on six different commercial particle types (three fully porous and three porous-shell particles) using the same test analyte (methylparaben), some significant differences in B-term band broadening could be observed. These differences change in magnitude with the analyte retention factor k', but nevertheless persist over the full range of considered k'-values ($1 < k' < 16$). The difference is most pronounced in the range between $k' = 3$ and $k' = 6$. In this range, the two porous-shell particles with the lowest B-term constant (Halo and Kinetex-particles) had a B-term constant (or effective longitudinal diffusion coefficient D_{eff}) that is about 50% smaller than the fully porous particle type with the highest B-term constant (Acquity particles). The other investigated materials (Poroshell, Zorbax 3.5 μm and Eclipse 1.8 μm) gave intermediate results. Considering that the presence of the solid core can only be expected to induce a 10–15% reduction of the B-term diffusion, the remaining differences must be due to differences in the porous zone diffusion coefficient. Indeed, analyzing the obtained B-term constant values using the EMT-expressions for longitudinal diffusion, the observed differences in B-term band broadening could be attributed to differences in meso-pore diffusion (γ_{mp}-value) and diffusion in the stationary phase ($\gamma_s D_s$-value). In general, these differences can be linked to notable differences in the structure of the meso-porous material, with the material with the largest pores and the largest internal porosity also leading to the largest γ_{mp}- and $\gamma_s D_s$-value, and vice versa.

References

[1] J. Kirkland, Anal. Chem. 64 (1992) 1239.
[2] J. Kirkland, F. Truszkowski, R. Ricker, J. Chromatogr. A 965 (2002) 25.
[3] A. Cavazzini, F. Gritti, K. Kaczmarski, N. Marchetti, G. Guiochon, Anal. Chem. 79 (2007) 5972.
[4] Y. Zang, X. Wang, P. Mukherjee, P. Petersson, J. Chromatogr. A 1216 (2009) 4597.
[5] E. Olah, S. Fekete, J. Fekete, K. Ganzler, J. Chromatogr. A 1217 (2010) 3642.
[6] D. Guillarme, J. Ruta, S. Rudaz, J.-L. Veuthey, Anal. Bioanal. Chem. 397 (2010) 1069.
[7] A. Felinger, J. Chromatogr. A 1218 (2011) 1939–1941.
[8] F. Gritti, A. Cavazzini, N. Marchetti, G. Guiochon, J. Chromatogr. A 1157 (2007) 289.
[9] F. Gritti, I. Leonardis, J. Abia, G. Guiochon, J. Chromatogr. A 1217 (2010) 1589.
[10] J.H. Knox, J. Chromatogr. A 831 (1999) 3.
[11] F. Gritti, I. Leonardis, J. Abia, G. Guiochon, J. Chromatogr. A 1217 (2010) 3819.
[12] K. Usher, C. Simmons, J. Dorsey, J. Chromatogr. A 1200 (2008) 122.
[13] K. Unger, R. Skudas, M. Schulte, J. Chromatogr. A 1184 (2008) 393.
[14] J.H. Knox, L. McLaren, Anal. Chem. 36 (1964) 1477.
[15] J.H. Knox, H.P. Scott, J. Chromatogr. 282 (1983) 297.
[16] K. Miyabe, Y. Matsumato, G. Guiochon, Anal. Chem. 79 (2007) 1970.
[17] K. Miyabe, N. Ando, G. Guiochon, J. Chromatogr. A 1216 (2009) 4377.
[18] F. Gritti, G. Guiochon, J. Chromatogr. A 1166 (2007) 30.
[19] F. Gritti, G. Guiochon, J. Chromatogr. A 1169 (2007) 125.
[20] R. Landauer, J. Appl. Phys. 23 (1952) 779.
[21] H.T. Davis, J. Am. Ceram. Soc. 60 (1977) 499.
[22] C. Maxwell, Treatise on Electricity and Magnetism, vol. 1, Oxford University Press, London, 1873.
[23] J. Sax, J.M. Ottino, Polym. Eng. Sci. 23 (1983) 165.
[24] C.M. Zimmerman, A. Singh, W.J. Koros, J. Membr. Sci. 137 (1997) 145.
[25] L. Rayleigh, Philos. Mag. 34 (1892) 481.
[26] D.A.G. Bruggeman, Ann. Phys. 416 (1935) 636.
[27] J. Crank, The Mathematics of Diffusion, 2nd ed., Clarendon Press, Oxford, 1975.
[28] E.L. Cussler, Diffusion. Mass Transfer in Fluid Systems, Cambridge University Press, Cambridge, UK, 1984.
[29] M. Barrande, R. Bouchet, R. Denoyel, Anal. Chem. 79 (2007) 9115.
[30] G. Desmet, K. Broeckhoven, J. De Smet, S. Deridder, G. Baron, P. Gzil, J. Chromatogr. A 1188 (2008) 171.
[31] G. Desmet, S. Deridder, J. Chromatogr. A 1218 (2011) 32.
[32] H. Kobayashi, D. Tokuda, J. Ichimaru, T. Ikegami, K. Miyabe, N. Tanaka, J. Chromatogr. A 1109 (2006) 2.
[33] F. Gritti, G. Guiochon, Chem. Eng. Sci. 61 (2006) 7636.
[34] F. Gritti, G. Guiochon, Anal. Chem. 78 (2006) 5329.
[35] F. Gritti, G. Guiochon, AIChE J. (2010), doi:10.1002/aic.1228099.
[36] S. Deridder, G. Desmet, J. Chromatogr. A 1218 (2011) 46.
[37] S. Torquato, J. Appl. Phys. 58 (1985) 3790.
[38] S. Torquato, Random Heterogeneous Materials, Springer Science & Business Media, New York, 2002.
[39] D. Cabooter, F. Lynen, P. Sandra, G. Desmet, J. Chromatogr. A 1157 (2007) 131.
[40] A. Liekens, D. Cabooter, J. Denayer, G. Desmet, J. Chromatogr. A 1217 (2010) 6754.
[41] J. Li, P. Carr, Anal. Chem. 69 (1997) 2530.
[42] J. Li, P. Carr, Anal. Chem. 69 (1997) 2550.
[43] C. Wilke, P. Chang, AIChE J. (1955) 264.
[44] G. Guillarme, S. Heinish, J.L. Rocca, J. Chromatogr. A 1052 (2004) 39.
[45] R.C. Reid, J.M. Prausnitz, B.E. Poling (Eds.), The Properties of Gases and Liquids, Mc Graw-Hill, London, UK, 1986.
[46] H. Guan, G. Guiochon, J. Chromatogr. A 731 (1996) 27.
[47] Y. Yao, A.M. Lenhoff, J. Chromatogr. A 1126 (2006) 107.
[48] Y. Yao, A.M. Lenhoff, J. Chromatogr. A 1037 (2004) 273.
[49] D. Lubda, W. Lindner, M. Quaglia, C. Du Fresne von Hohenesche, K. Unger, J. Chromatogr. A 1083 (2005) 14.
[50] K. Miyabe, G. Guiochon, J. Chromatogr. A 1217 (2010) 1713.
[51] R. Bujalski, F. Cantwell, Anal. Chem. 78 (2006) 1593.
[52] J. Giddings, Dynamics of Chromatography. Part I: Principles and Theory, Dekker, New York, 1965.
[53] C.A. Miller, S. Torquato, J. Appl. Phys. 68 (1990) 5486.
[54] V. Silva, P. Prádanos, L. Palacio, J.I. Calvo, A. Hernández, Chem. Eng. J. 149 (2009) 78.
[55] P. Dechadilok, W.M. Deen, Ind. Eng. Chem. Res. 45 (2006) 6953.
[56] K. Broeckhoven, D. Cabooter, F. Lynen, P. Sandra, G. Desmet, J. Chromatogr. A 1188 (2008) 189.
[57] R.W. Stout, J.J. Destefano, L.R. Snyder, J. Chromatogr. 282 (1983) 263.